Available online at www.sciencedirect.com
SCIENCE DIRECT®

Journal of the European Ceramic Society 24 (2004) 2433–2443

www.elsevier.com/locate/jeurceramsoc

Reaction mechanisms and kinetics of the synthesis and decomposition of lithium metazirconate through solid-state reaction

Heriberto Pfeiffer, Kevin M. Knowles*

University of Cambridge, Department of Materials Science and Metallurgy, Pembroke Street, Cambridge CB2 3QZ, UK

Received 8 February 2003; received in revised form 19 June 2003; accepted 22 June 2003

Abstract

The reaction mechanisms and kinetics describing the formation and surface decomposition of lithium metazirconate pellets (Li_2ZrO_3) have been investigated during Li_2ZrO_3 formation via solid-state reaction. Samples were analysed by X-ray diffraction, scanning electron microscopy and transmission electron microscopy. A metastable tetragonal Li_2ZrO_3 phase was synthesised at low temperatures, recrystallizing into a monoclinic structure when the temperature was increased above 800 °C. Prolonged heat treatment at 900 °C showed that Li_2ZrO_3 pellets were stable at this temperature for up to 3 h. For longer heat treatments at 900 °C, Li_2ZrO_3 lost Li_2O from the surface of the pellets, decomposing to ZrO_2. Similar, more rapid, decomposition behaviour was found at higher temperatures. Pellets heated for 48 h at 1100 °C produced a 170 μm thick ZrO_2 layer on the surface of the pellets. Modelling the loss of lithium oxide from Li_2ZrO_3 in terms of a diffusion-controlled model, the activation energy for this decomposition of Li_2ZrO_3 to ZrO_2 was estimated to be 210 kJ mol^{-1}.

Keywords: Diffusion; Li_2ZrO_3; Nuclear applications; Powders-solid state reaction; X-ray methods

1. Introduction

Lithium ceramics are of research interest because of their technological applications. Thus, for example, there has been research in recent years on their application as electronic devices and as breeder materials for nuclear fusion reactors, in addition to other more well-known applications such as in batteries and in low thermal expansion glass-ceramics used in ceramic hobs.[1–7] Lithium aluminate ($LiAlO_2$), lithium silicates (e.g., Li_2SiO_3, $Li_2Si_2O_5$ and Li_4SiO_4) and lithium zirconates (e.g., Li_2ZrO_3 and $Li_6Zr_2O_7$) are candidate materials in nuclear research as tritium (^3T) breeding materials.[8–11] Such ceramics enable the reaction:

$$^6Li + n_t \rightarrow {}^3T + {}^4He \quad (1)$$

to be exploited.[12]

Lithium metazirconate (Li_2ZrO_3) has been proposed as a good candidate breeding material because of its high potential to produce tritium.[13] Although Li_2ZrO_3 has a moderate tritium release and exhibits good irradiation characteristics,[6,10] there is relatively little work reported on the synthesis and thermal stability of this compound. There is agreement in the literature that Li_2ZrO_3 exhibits two different polymorphs, one, *m*-Li_2ZrO_3, with a monoclinic crystal structure with $a = 5.43$ Å, $b = 9.02$ Å, $c = 5.41$ Å and $\beta = 112.16°$ and the other, *t*-Li_2ZrO_3, with a tetragonal crystal structure with $a = 9.0$ Å and $c = 3.43$ Å.[14–17] It is also recognized that the monoclinic polymorph, *m*-Li_2ZrO_3, is the stable polymorph. The melting temperature of the monoclinic polymorph has been variously estimated to be 1600 ± 50 °C[15] and 1695 ± 15 °C.[16] Li_2ZrO_3 can be synthesized successfully from Li_2O and ZrO_2 powder mixtures and Li_2CO_3 and ZrO_2 powder mixtures,[16] as well as via crystallization of an amorphous powder produced by gelling zirconium propylate and lithium acetate.[10] It is apparent from the literature that the choice of processing route determines the efficiency of conversion to the monoclinic polymorph.[10,16]

The aim of the work reported here was to study in detail the Li_2CO_3 and ZrO_2 powder mixture route for the production of relatively low density (60–70% theoretical density) Li_2ZrO_3 pellets. To achieve this, we have used X-ray diffraction, scanning electron microscopy and transmission electron microscopy to monitor

* Corresponding author. Tel.: +44-1223-334312; fax: +44-1223-334567.
E-mail address: kmk10@cam.ac.uk (K.M. Knowles).

0955-2219/$ - see front matter © 2003 Elsevier Ltd. All rights reserved.
doi:10.1016/S0955-2219(03)00630-7

reaction progress as a function of heat treatment temperature and time.

2. Experimental procedure

Stoichiometric amounts of lithium carbonate (Li_2CO_3, Aldrich) and zirconium oxide (ZrO_2, Aldrich), all of reagent-grade purity, were ball-milled for 20 h with water, using zirconia balls as the dispersion agent. The powders were dried, pulverised and cold pressed into 10 mm-diameter pellets under a pressure of 10 t before reaction. These pellets were typically 2 mm thick. The pellets were heated in an electrical furnace for various temperatures and times. First, a set of samples was heat treated for 4 hrs at temperatures between 500 and 1000 °C. Each sample was placed in the furnace directly after the appropriate heat treatment temperature had been obtained. Subsequently, sets of samples were heat treated between 900 °C and 1050 °C for different times. After heat treatment, the samples were removed from the furnace and air-cooled to room temperature.

Thermogravimetric analysis (TGA) was performed with a heating rate of 10 °C min^{-1} in a TGA 51 Thermogravimetric Analyzer. The composition and morphology of the pellets were identified by X-ray diffraction (XRD), scanning electron microscopy (SEM) and transmission electron microscopy (TEM). A diffractometer (Philips, PW-1710) coupled to a copper-anode X-ray tube was used for XRD. The Cu$K_{\alpha 1}$ wavelength was selected with a diffracted beam monochromator. The relative percentages of the various compounds present in the pellets were estimated semi-quantitatively from the total area under the most intense diffraction peak for each phase identified, with the simplifying assumption this was proportional to the volume fraction of each compound. In this way, the amounts of the crystalline compounds present in the samples were obtained within an estimated experimental error of ±5%; this estimate arises from a comparison of the estimates obtained on two phase mixtures of Li_2ZrO_3 and ZrO_2 using this method and using the more quantitative X'Pert Plus software.

The particle size and morphology of the pellets were studied by SEM and TEM. Samples for SEM were covered with gold to overcome their lack of electrical conductivity and then analysed in a JEOL microscope (JSM-5800 LV). Samples for TEM were prepared using standard methods and the samples were examined in a Jeol 200CX transmission electron microscope at 200 kV.

3. Results and discussion

A TGA curve from room temperature to 900 °C for the dried powder mixture after ball-milling is shown in Fig. 1. A dramatic reduction of weight loss is shown between ~600 and 750 °C, with the rate of weight loss being most great at 720 °C. The overall weight loss was 23% of the initial weight. It is well known that Li_2CO_3 decomposition to Li_2O and CO_2 occurs at 710 °C,[2] but a further possibility here is that CO_2 loss occurs in parallel with a chemical reaction between Li_2CO_3 and ZrO_2:

$$Li_2CO_3 + ZrO_2 \rightarrow Li_2ZrO_3 + CO_2(g) \quad (2)$$

For this reaction, $\Delta G^\circ = -1650 + 0.2492T$ kJ mol^{-1}, where 1332 K $\leqslant T \leqslant$ 1642 K.[17]

In order to establish the reaction mechanism, samples were heat treated for 4 h between 500 and 1000 °C at 100 °C intervals. XRD results from the surfaces of the pellets before heat treatment and after various heat treatments are shown in Fig. 2. The XRD patterns of the samples at room temperature and 500 °C only show the presence of ZrO_2 and Li_2CO_3 (JCPDS file nos. 86-1450 and 87-0729 respectively). It is apparent that the ZrO_2 diffraction pattern from all the samples at 500 °C and above have much stronger 111 peaks at $2\theta = 31.473^\circ$ than might be expected from the JCPDS file no. 86-1450.[18] By contrast, X-ray diffraction from pulverised slices taken from the surface regions of the pellets heat treated at 500 °C and above all showed the expected JCPDS pattern for monoclinic zirconia. Thus, the difference between the diffractometer traces for zirconia and the JCPDS standard for monoclinic zirconia seen in Fig. 2 can be attributed to the experimental set-up we have used. In general, this can arise either from the sampling of a finite number of surface grains by the X-ray beam or from a textural effect in the sample. As we will demonstrate later in this paper, the latter explanation is consistent with SEM microstructural observations we have made subsequently on the pellets.

A small amount (12%) of *t*-Li_2ZrO_3 (JCPDS file no. 20-0647)[14] could be detected in the surface of the sample heat treated for 4 h at 600 °C, the remainder of the pellet surface being ZrO_2 (68%) and Li_2CO_3 (20%). No

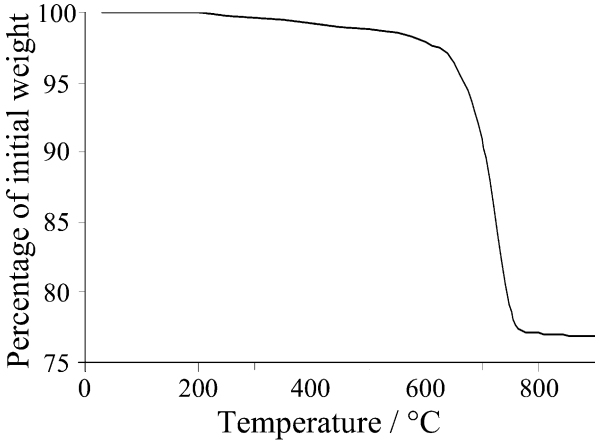

Fig. 1. Thermogravimetric analysis of starting materials for Li_2ZrO_3 synthesis.

evidence was found in this or any other sample for the metastable tetragonal Li_2ZrO_3 polymorph with $a = 4.26$ Å and $c = 9.014$ Å reported by Quintana et al.[19] Increasing the heat treatment temperature to 700 °C caused a dramatic change in the composition of the pellet surfaces. Analysis of the XRD diffractometer pattern showed that the sample surface was 72% *t*-Li_2ZrO_3, 8% ZrO_2, 8% $Li_6Zr_2O_7$ (JCPDS file no. 36-0122) and 12% *m*-Li_2ZrO_3 (JCPDS file no. 76-1150), indicating that, within the limits of detectability, Li_2CO_3 had totally decomposed. The formation of $Li_6Zr_2O_7$ is consistent with heterogeneities in the pellet surface arising from chemical reaction between ZrO_2 and Li_2CO_3: some parts of the pellet will be locally richer in lithium than the average, enabling $Li_6Zr_2O_7$ to form, while at the same time leaving unreacted ZrO_2 elsewhere in the pellet. Others have also reported the formation of $Li_6Zr_2O_7$ at 700 °C in powder mixtures of Li_2CO_3 and ZrO_2 and Li_2O and ZrO_2.[16]

Increasing the heat treatment temperature to 800 °C, 900 °C and 1000 °C changed the relative proportions of the four phases, *m*-Li_2ZrO_3, *t*-Li_2ZrO_3, $Li_6Zr_2O_7$ and ZrO_2, found on the surface of the pellets, as shown in Fig. 3. The proportion of $Li_6Zr_2O_7$ declined to zero as the temperature increased. $Li_6Zr_2O_7$ can either decompose or react with zirconia through the chemical reactions:

$$Li_6Zr_2O_7 \rightarrow 2Li_2ZrO_3 + Li_2O \quad (3)$$

and

$$Li_6Zr_2O_7 + ZrO_2 \rightarrow 3Li_2ZrO_3. \quad (4)$$

Significantly, pure Li_2ZrO_3 was not obtained in any of these heat treatments. The highest content of *m*-Li_2ZrO_3 (81%) was found in the sample heat treated for 4 h at 900 °C. The replacement of *t*-Li_2ZrO_3 by *m*-Li_2ZrO_3 as the temperature increased agrees with previous work.[16] When the sample was heated for 4 h at 1000 °C, the proportion of *m*-Li_2ZrO_3 declined while that of ZrO_2 increased. This is consistent with loss of lithium from the pellet surface in the form of Li_2O, for example through a decomposition reaction such as:

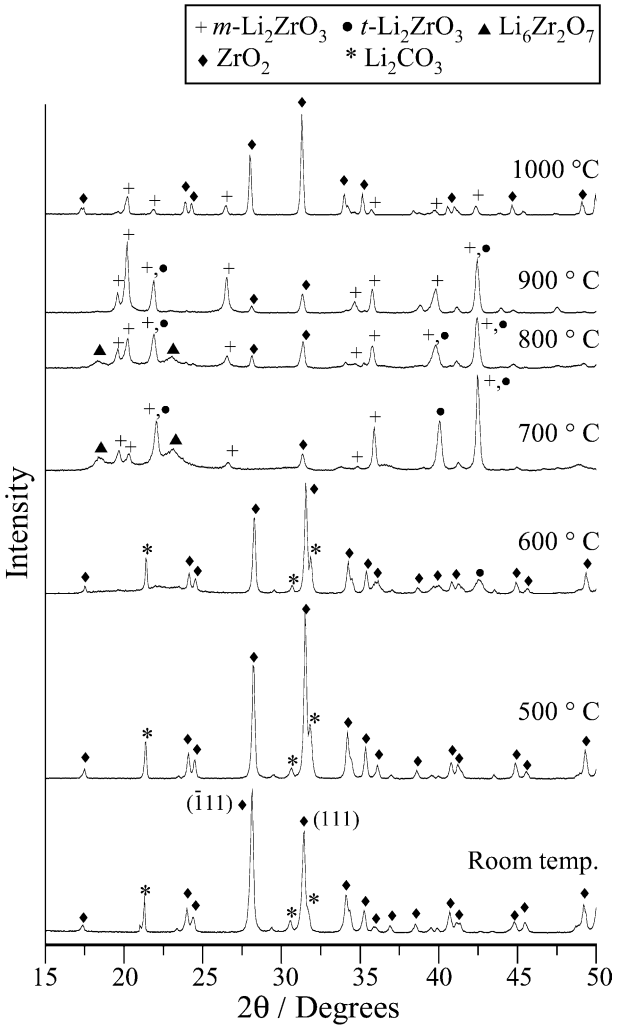

Fig. 2. X-ray diffraction patterns of the pellets heat treated for 4 h at different temperatures.

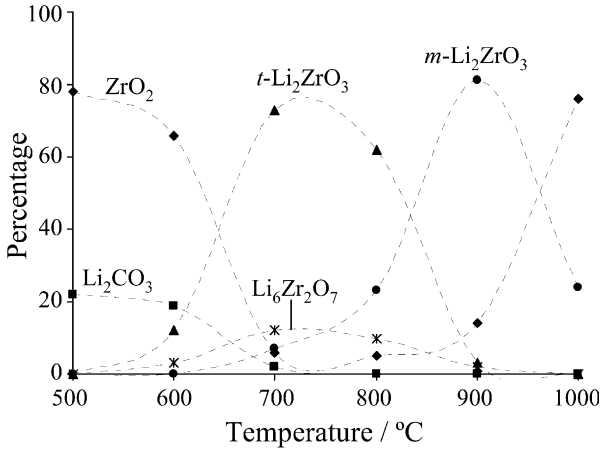

Fig. 3. Percentage of Li_2CO_3, ZrO_2, *t*-Li_2ZrO_3, *m*-Li_2ZrO_3 and $Li_6Zr_2O_7$ as a function of temperature.

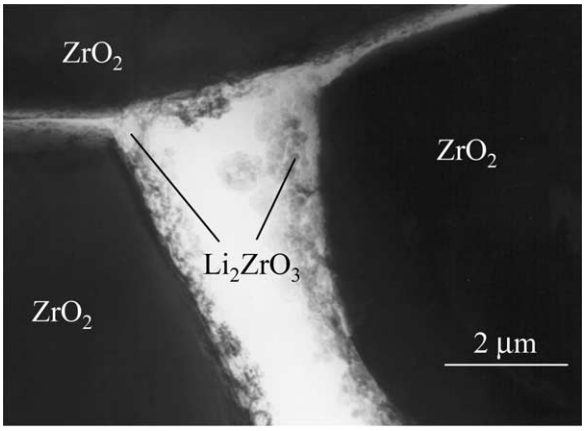

Fig. 4. Bright-field TEM image of ZrO_2 particles surrounded by *m*-Li_2ZrO_3.

$$Li_2ZrO_3 \rightarrow ZrO_2 + Li_2O \quad (5)$$

This lithium loss is also compatible with reports in the literature that Li_2O is irreversibly lost from some lithium ceramics when they are heated at temperatures higher than 900 °C.[16,20–22]

The lithium metazirconate pellets produced during the first set of heat treatments for 4 h at temperatures between 700 and 1000 °C all consist of ZrO_2, $Li_6Zr_2O_7$, *m*-Li_2ZrO_3 and *t*-Li_2ZrO_3. In general, TEM of these samples showed that they all exhibited a microstructure in which Li_2ZrO_3 was found growing on the surface of a different phase, typically ZrO_2. This effect is shown in Fig. 4, a bright-field TEM image taken from the sample heat treated at 700 °C for 4 h. Particles of ZrO_2 surrounded by small particles of *m*-Li_2ZrO_3 are clearly shown in this micrograph.

According to Wyers and Cordfunke,[16] *m*-Li_2ZrO_3 is stable between 800 and 1500 °C. However, in our work it was apparent that *m*-Li_2ZrO_3 started to decompose at 900 °C. This behaviour can be explained in terms of the different stabilities of *m*-Li_2ZrO_3, depending on whether the sample is in the form of a pellet or simply as powder. The interparticle transfer of matter, which takes place in pellets during sintering, could enable Li_2O to evaporate at lower temperatures. Points of high surface curvature, such as necks between particles, are sites of increased vapour pressure.[23] If this were to be the case, it would suggest that the decomposition of *m*-Li_2ZrO_3 would be more likely to occur at the surface of a pellet rather than within its interior.

To examine this hypothesis, pure *m*-Li_2ZrO_3 was prepared using excess lithium carbonate in the starting composition. Specifically, for every mole of ZrO_2, 1.05 moles of Li_2CO_3 were used in the formulation. The powders were heat treated at 900 °C for 3 h. XRD of the powders showed only *m*-Li_2ZrO_3. Pellets were prepared from the pure *m*-Li_2ZrO_3 at room temperature by uniaxial cold pressing. These pellets were subsequently heat treated between 900 and 1100 °C for different times. XRD patterns from the surfaces of the pellets were obtained after each heat treatment. The pellets were then ground down and polished. XRD patterns were once again obtained from the new surfaces. This procedure was done several times. The percentages of ZrO_2 found at the different depths in the pellet are shown in Fig. 5. There is a clear trend showing that the amount of ZrO_2 decreases as the distance from the original surface increases. This suggests strongly that Li_2ZrO_3 decomposition does indeed occur preferentially in the surface of the pellets.

SEM micrographs of the Li_2ZrO_3 pellets heated at 900 °C for 30 min and 420 min are shown in Fig. 6. The grain size was measured using standard procedures,[24] and, as expected, there was significant grain growth between 30 min at 900 °C and 420 min at 900 °C. After 30 min, the particles are rather small, polygonal particles with a size between 1 and 2 μm. Although the shape of the particles did not change after 420 min of thermal treatment, the size of the particles increased from 2 to 5 μm. When samples were heated at 1100 °C for different

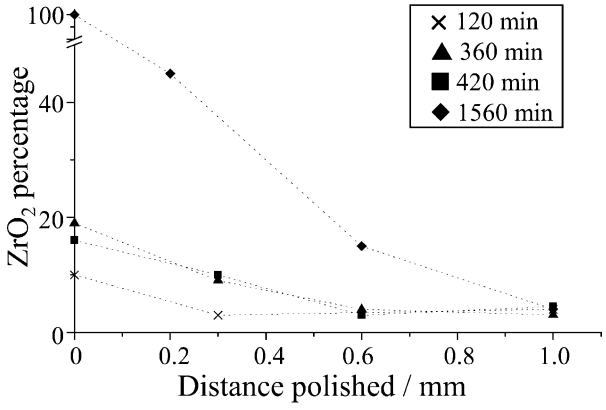

Fig. 5. ZrO_2 percentage as a function of the depth into the pellets heat treated at 900 °C for different times.

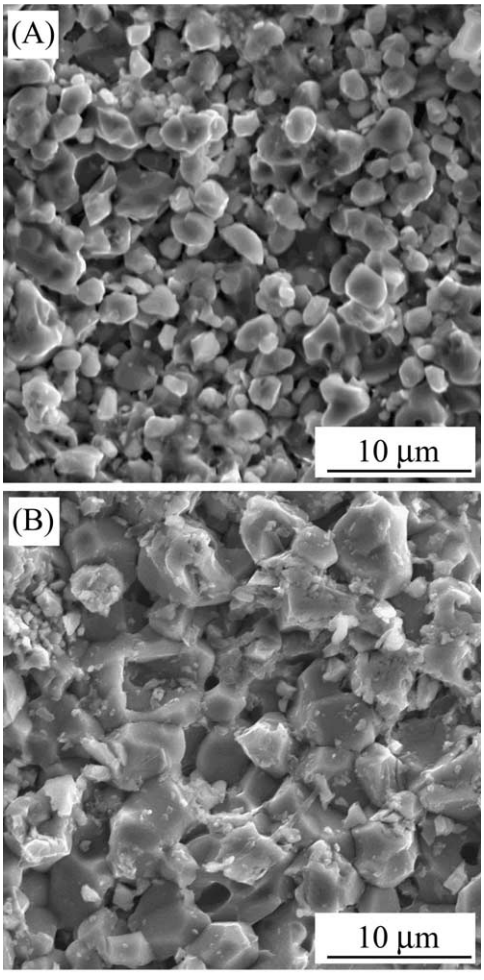

Fig. 6. SEM micrographs of the Li_2ZrO_3 pellets heat treated at 900 °C. (A) Li_2ZrO_3 pellet heat treated for 30 min and (B) Li_2ZrO_3 pellet heat treated for 420 min.

times, grain growth was also observed (Fig. 7). However, the surface of the samples heated at 1100 °C for 420 min became noticeably more rough in appearance [Fig. 7(B)]. From XRD, samples heated at 1100 °C for 420 min were found to contain 60% ZrO_2 in the surface region.

To examine the proposition that the change in surface morphology seen in Fig. 7(B) arose from the formation of ZrO_2 as a result of Li_2ZrO_3 decomposition, a Li_2ZrO_3 pellet was heat treated at 1100 °C for 48 h. SEM micrographs of different parts of the pellet are shown in Fig. 8. Although lithium could not be detected by EDX because of its low atomic number, the backscattered electron image (BSEI) in Fig. 8(A) confirms the presence of two phases in the surface region. The difference in contrast seen in Fig. 8(A) arises from the differences in mean atomic number, $\overline{Z}$, of Li_2ZrO_3 ($\overline{Z}=11.67$) and ZrO_2 ($\overline{Z}=18.67$), giving rise to a difference in the backscattered electron coefficient, η, of the two phases through the equation[25]

$$\eta = -0.0254 + 0.016\overline{Z} - 1.86 \times 10^{-4}\overline{Z}^2 + 8.3 \times 10^{-7}\overline{Z}^3 \quad (6)$$

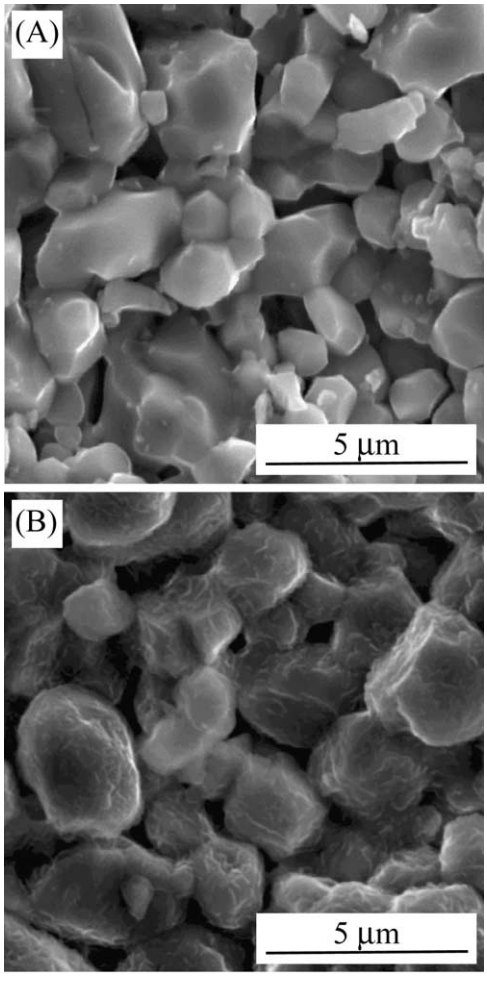

Fig. 7. SEM micrographs of the Li_2ZrO_3 pellets heat treated for 420 min at different temperatures. (A) Li_2ZrO_3 pellet heat treated at 900 °C and (B) Li_2ZrO_3 pellet heat treated at 1100 °C.

η decreases from 0.213 for ZrO_2, the lighter phase in Fig. 8(A) to 0.137 for Li_2ZrO_3, the darker phase.

Although the Li_2ZrO_3 phase remains as polygonal particles, the mean particle size after sintering at 1100 °C for 48 h increased to 60±10 μm. Furthermore, the

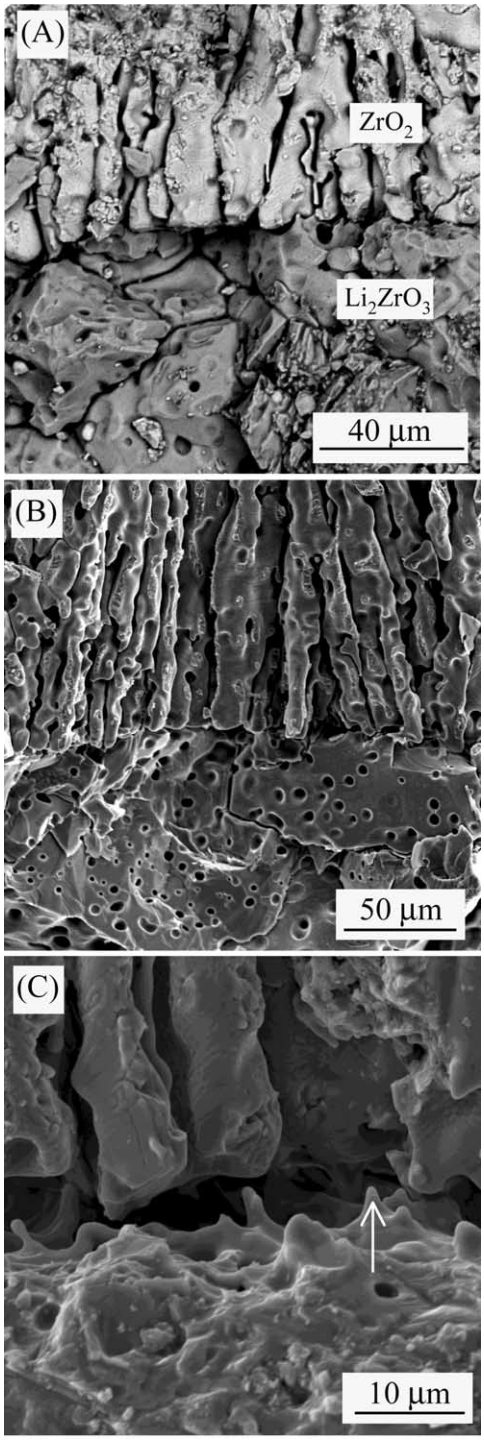

Fig. 8. SEM micrographs of different parts of a Li_2ZrO_3 pellet heat treated at 1100 °C for 48 h. (A) BSEI at the interface between Li_2ZrO_3 and surface ZrO_2. (B) Secondary electron image of the same region. (C) Secondary electron image showing detail of the Li_2ZrO_3–ZrO_2 interface. A needle-like ZrO_2 particle is arrowed.

particles contained large pores that were not present after shorter heat treatment times (Figs. 6 and 7). By contrast, the ZrO_2 surface region had a distinctive columnar growth morphology reminiscent of a grain structure frequently observed in thin films.[26] The thickness of this ZrO_2 external layer after 48 h was 170 ± 20 μm. Not surprisingly, X-ray diffractometer examination of the surface of this pellet after this extended heat treatment only showed peaks from *m*-ZrO_2. Close examination of the Li_2ZrO_3-ZrO_2 interface shows that small needle-like particles of ZrO_2 are growing in the surface of the Li_2ZrO_3 particles [Fig. 8(C)]. These small needles act as nucleation centres for the columnar ZrO_2 grains. The origin of the 'anomalous' XRD diffraction patterns from ZrO_2 in Fig. 2 can be therefore attributed to the way in which the ZrO_2 nucleates and grows in the presence of Li_2ZrO_3, introducing a texture into the surface ZrO_2, an extreme example of which after prolonged heat treatment is demonstrated in Fig. 8.

In order to establish the reaction mechanism and the decomposition mechanism of Li_2ZrO_3 during the solid-state reaction in more detail, a further batch of pellets were heat-treated for different heating times at 900, 950, 1000 and 1050 °C. The results of X-ray diffraction from the surfaces of pellets heat-treated at 900 °C for less than 1 h and 1 h or more are shown in Figs. 9 and 10 respectively. It is apparent from Fig. 9 that when the samples were cooled down after 20 min of heat treatment or less, multiphase mixtures containing Li_2CO_3, ZrO_2, *t*-Li_2ZrO_3, *m*-Li_2ZrO_3 and $Li_6Zr_2O_7$ were found. Li_2CO_3 and $Li_6Zr_2O_7$ disappeared from the X-ray diffractometer traces after 5 min and 20 min of heat treatment respectively, and *t*-Li_2ZrO_3 disappeared after 40 min. The highest content of *m*-Li_2ZrO_3 was observed when samples had been heat treated between 1 and 3 h. After 3 h or more at 900 °C, the amount of ZrO_2 detected on the X-ray diffractometer traces increased, up to 45% of the total sample analysed after 10 h at 900 °C. As a consequence of this, the Li_2ZrO_3 content decreased (Fig. 10). The estimated percentages of the different compounds present in the samples during the heat treatment at 900 °C are summarized in Fig. 11.

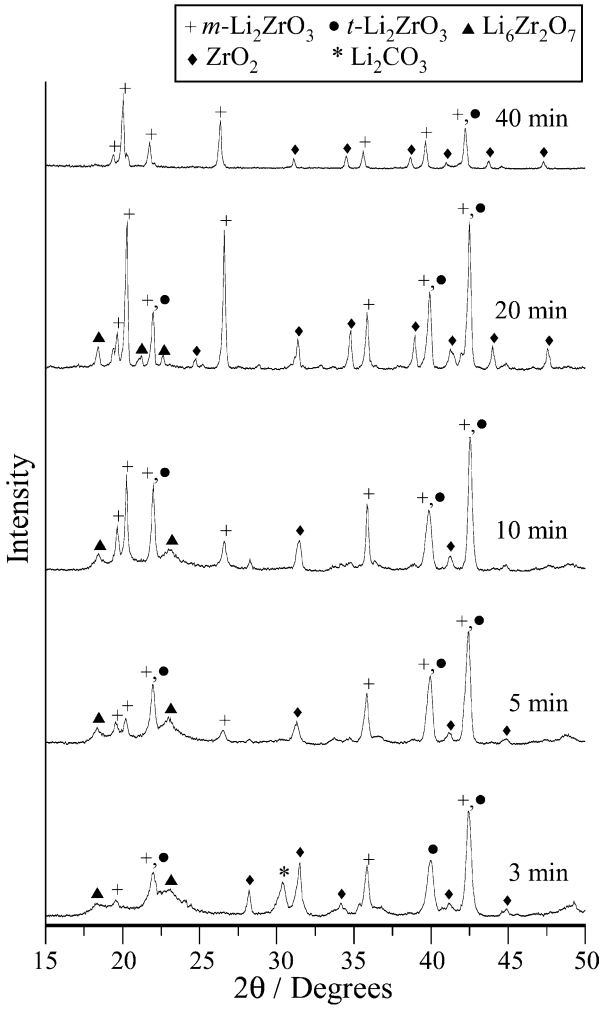

Fig. 9. X-ray diffraction patterns of samples heat treated at 900 °C for times less than one hour.

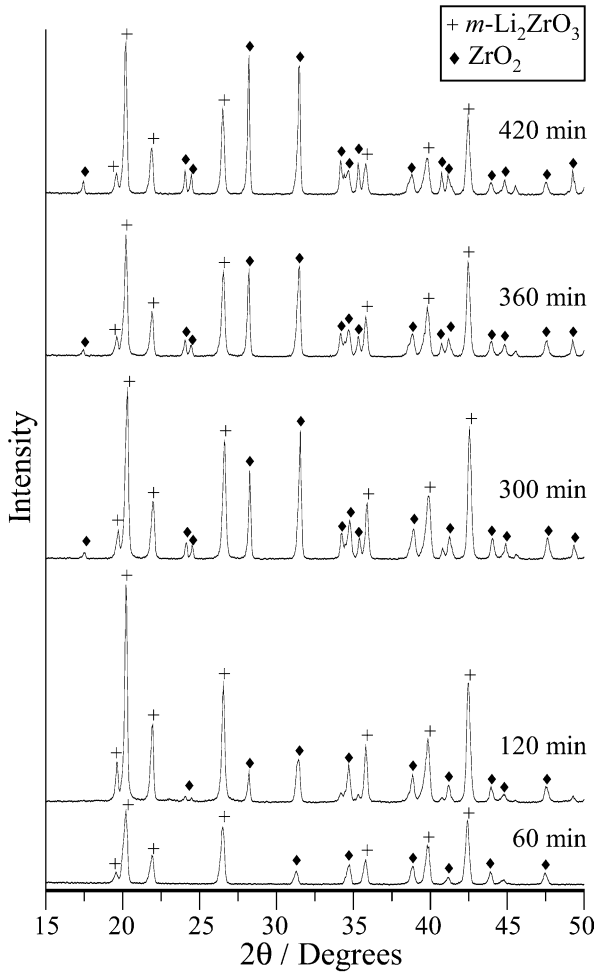

Fig. 10. X-ray diffraction patterns of samples heat treated at 900 °C for times of one hour or more.

Samples heat-treated at 950, 1000 and 1050 °C presented similar behaviour to the samples heat treated at 900 °C, but the increase in temperature led to more rapid reaction kinetics. Thus, for example, in samples heat treated at 900 °C, the amount of ZrO_2 decreased to 8% after 60 min and increased again after 180 min, with a 2 h lag period within which the composition of the pellet was essentially invariant. The final amount of ZrO_2 was 40% after 600 min. At 950 °C, the lag period was shorter, only 60 min, beginning after 30 min of heat treatment. The amount of ZrO_2 in this lag phase was ~12%. The decomposition of Li_2ZrO_3 produced 55% of ZrO_2 after 400 min at 950 °C. For samples studied at 1000 °C, the minimum amount of ZrO_2 was 12% at 30 min and the lag period disappeared. In this case, the steady growth in the amount of ZrO_2 began after 30 min of heating time and the final ZrO_2 percentage was 75%. Finally, at 1050 °C, the results were very similar to those at 1000 °C. Hence, raising the reaction temperature decreases the lag period where the Li_2ZrO_3 is stable, and increases the ZrO_2 reconversion ratio. The relationship between the percentage of ZrO_2 present and time spent at temperature is shown in Fig. 12.

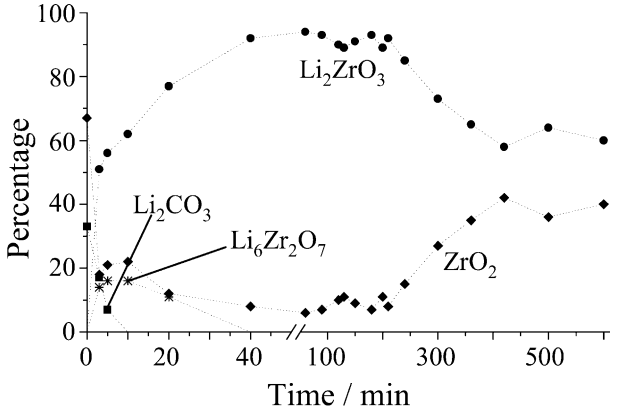

Fig. 11. Percentage of Li_2CO_3, ZrO_2, Li_2ZrO_3 and $Li_6Zr_2O_7$ as a function of time at 900 °C.

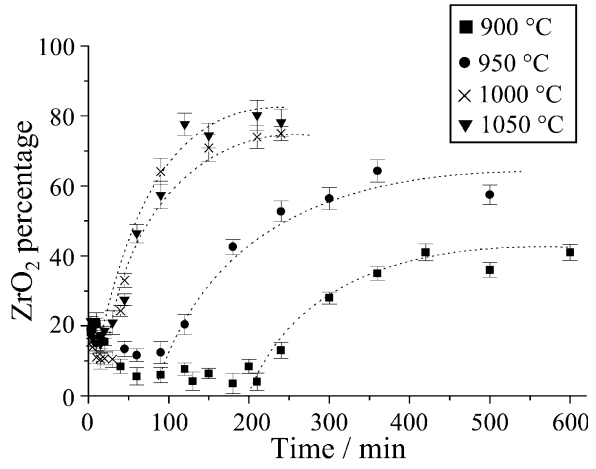

Fig. 12. Relationship between ZrO_2 conversion ratio and time during isothermal heating at different temperatures.

An examination of the decomposition of Li_2ZrO_3 to ZrO_2 showed, that in the first few hours of the reaction (i.e., for the conditions we have examined), the rate of reaction in the surface regions of the pellets could be described adequately well mathematically in terms of a diffusion reaction controlled by movement of an interface. Since the pellets were 10 mm in diameter and 1–2 mm thick, the appropriate model to use is that of one-dimensional diffusion, so that the reaction mechanism follows an equation of the form

$$x^2 = 2D(t - t_0) \tag{7}$$

where x is the thickness of ZrO_2 on the circular surface of the pellets at time t. To take account of the experimental observations of a lag period before the development of the ZrO_2 layer, it is assumed in this model that growth of the ZrO_2 layer does not begin until a time t_0 has elapsed during the heat treatment.

In order to relate this diffusion model to the data for the conversion ratio to ZrO_2 in Fig. 12 measured by X-rays, the nature of the way in which X-rays interact with the specimens has to be considered. A simple treatment of this is given in the Appendix. From Eq. (a.8) it is apparent that as x increases, the ratio of the intensity of strong, easily identifiable, X-ray diffraction peaks from ZrO_2 and Li_2ZrO_3 will increase, so that the apparent volume fraction of ZrO_2 determined from the X-ray diffractometer trace will increase.

A short computer program was written to determine the apparent level of ZrO_2 as a function of x for initial bulk compositions of the pellets representative of the compositions at the end of the lag periods for each of the four temperatures in Fig. 12. Thus, from the data in Fig. 12, thicknesses, x, as a function of time, t, could be obtained. For these calculations, it was assumed that the ZrO_2 surface layer had 40 vol.% porosity and that the bulk pellets had 35 vol.% porosity. Hence, the linear absorption coefficient of the ZrO_2 surface layer was taken to be 369 cm^{-1}, and so the distance an X-ray would have to travel in this layer for its intensity to be attenuated by a factor of e is 27 μm.

Plotting x^2 against t produces the data in Fig. 13. It should be noted that the absolute values of x predicted from this analysis for the data in Fig. 12 were small, of the order of a few micrometres. Despite the high level of noise in the data in Fig. 13 it is apparent that as the temperature increases, the gradients of the best-fit lines all increase.

For a diffusional growth model, the gradients of these best-fit lines are all proportional to the diffusion coefficient, D, at the temperature of interest. If these follow an Arrhenius-type behaviour so that

$$D = D_0 \exp(-Q/RT) \tag{8}$$

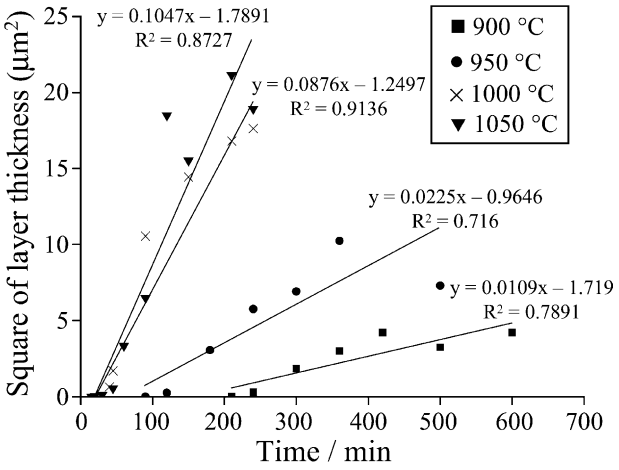

Fig. 13. Plot of x^2 against time for the growth of a thin surface layer of ZrO_2 on Li_2ZrO_3-rich pellets.

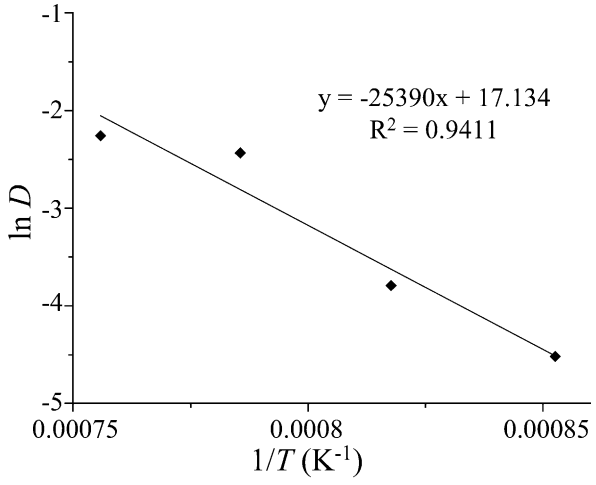

Fig. 14. Plot of ln D versus $1/T$ for the decomposition of Li_2ZrO_3 to ZrO_2.

where D_0 is the reaction rate constant, Q is the activation energy of the diffusion process, R is the gas constant and T is absolute temperature, a plot of ln D versus $1/T$ should be a straight line.

Such a plot is shown in Fig. 14, from which the activation energy for the decomposition of Li_2ZrO_3 to ZrO_2 can be estimated to be 210 kJ mol^{-1}. This is consistent with a solid state diffusion mechanism in which at these temperatures diffusion of lithium ions to the surface of the pellets is the rate-determining step in the decomposition of Li_2ZrO_3.

The absolute values of thickness of the zirconia layer predicted by this analysis as a function of time and temperature should be treated with some caution and should be regarded as back-of-the-envelope calculations rather than anything more quantitative. Given a predicted layer thickness of around 2 μm after 400 min at 900 °C, an activation energy of 210 kJ mol^{-1} would suggest a ZrO_2 layer of the order of 25 μm thick after heat treatment at 48 h at 1100 °C. This is substantially less than the thickness of 170 μm seen in Fig. 8. Nevertheless, this is not too unreasonable given the simplifying assumptions we have made in modelling the initial stages of growth of the ZrO_2 layer in terms of a growth of a uniform thin film on the surface of the pellets. Equally reasonable is the likelihood that the columnar growth morphology which has developed in the sample shown in Fig. 8 provides short circuit diffusion paths for lithium loss which speeds up the kinetics of the decomposition even more than might be expected. However, it is apparent that further, more detailed, work on how Li_2O is lost from Li_2ZrO_3 pellets is required.

4. Conclusions

Lithium metazirconate pellets were prepared by solid-state reaction using ZrO_2 and Li_2CO_3 as reactants. Temperature was found to be a very important factor in the reaction mechanism of Li_2ZrO_3 synthesis and its subsequent decomposition. ZrO_2 was present in the heat treated pellets arising either from the starting composition in pellets heat treated below 800 °C or from decomposition of the Li_2ZrO_3 for pellets heat treated at and above 900 °C. The conversion ratio of Li_2ZrO_3 was best at 900 °C, when the sample was heat treated for between 60 and 180 min. Pure samples of Li_2ZrO_3 could only be obtained with excess Li_2CO_3 in the starting composition. Li_2ZrO_3 decomposed when it was heat treated for longer times than 180 min at 900 °C. The same behaviour was observed for 950, 1000 and 1050 °C, the time of stability being less at these higher temperatures. Pellets heated for 48 h at 1100 °C produced a 170 μm thick layer of ZrO_2 on their surfaces. The activation energy for the Li_2ZrO_3 decomposition process was estimated to be 210 kJ mol^{-1}.

Acknowledgements

H. Pfeiffer thanks Consejo Nacional de Ciencia y Tecnología (CONACyT) and Secretaría de Educación Pública (SEP) from México, for partial financial support.

Appendix a. Absorption of the X-ray beam in a parafocusing diffractometer by a surface layer

In the parafocusing diffractometer, such as a Philips PW-1710 diffractometer, the sample is in the form of a flat plate and the incident and diffracted X-ray beams both make the same angle with the normal to the flat plate. If the sample is composed of a thin surface layer of thickness x underneath which there is bulk material,

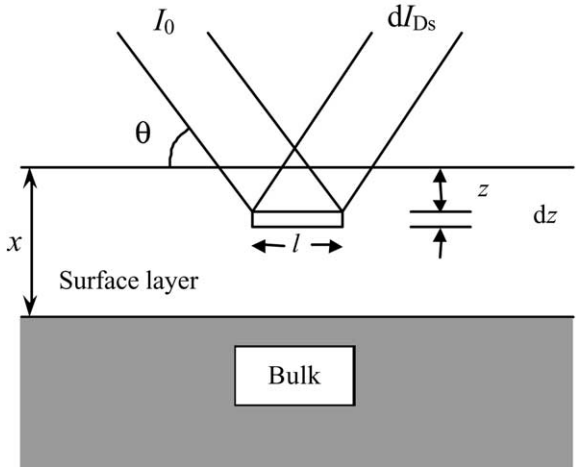

Fig. a1. Geometry of X-ray diffraction from a flat plate with a surface layer of thickness x. The incident and diffracted beams make the same angle θ with the normal to the plate and have unit width.

the relative intensities of X-rays from the bulk material will be reduced and the relative intensities of X-rays from the surface will be enhanced because of absorption.

This effect can be modelled quantitatively by a simple extension of the modelling of absorption of X-rays from an isotropic flat plate in the parafocusing diffractometer.[27] The relevant geometry is shown in Fig. a1. It is assumed that the incident X-ray beam is composed of parallel rays of intensity I_0 J m^{-2} s^{-1}. X-rays diffracted from an element at a depth z below the surface travel a total distance within the specimen of $2z$ csc θ before re-emerging.

For X-rays diffracted from the surface layer, $0 \leqslant z \leqslant x$, and so because of absorption, X-rays diffracted from the volume element $l\mathrm{d}z$ in Fig. a1 will have an integrated intensity

$$\mathrm{d}I_{Ds} = AlI_0 \exp(-2\mu_s z \csc\theta)\mathrm{d}z \tag{a.1}$$

In this equation, A takes into account the likelihood of particles or grains being in the correct orientation for diffraction and the fraction of incident energy diffracted by one unit volume and can be regarded as a constant.[27] The degree to which this part of the specimen absorbs X-rays is taken into account by the linear absorption coefficient, μ_s, of the surface layer. If the incident beam has unit width, $l = \csc\theta$, and so

$$\mathrm{d}I_{Ds} = A\csc\theta I_0 \exp(-2\mu_s z \csc\theta)\mathrm{d}z \tag{a.2}$$

The total diffracted intensity from the surface layer is obtained by integrating over the surface layer thickness:

$$I_{Ds} = A\csc\theta I_0 \int_0^x \exp(-2\mu_s z \csc\theta)\mathrm{d}z = \frac{AI_0}{2\mu_s}(1 - \exp(-2\mu_s x \csc\theta)) \tag{a.3}$$

For X-rays diffracted from the bulk material, $0 \leqslant x \leqslant z$. These X-rays travel a distance of $2x$ csc θ in the surface material and a distance $2(z-x)$ csc θ in the bulk material before re-emerging. In this case, X-rays diffracted from a volume element $l\mathrm{d}z$ will have an integrated intensity

$$\mathrm{d}I_{Db} = A\csc\theta I_0 \exp(-2\mu_s x \csc\theta - 2\mu_b(z-x)\csc\theta)\mathrm{d}z \tag{a.4}$$

where μ_b is the linear absorption coefficient in the bulk material.

The total diffracted intensity from a reflection from the bulk material is obtained by integrating z from x to ∞:

$$I_{Db} = A\csc\theta I_0 \exp(-2\mu_s x \csc\theta) \int_x^\infty \exp(-2\mu_b(z-x)\csc\theta)\mathrm{d}z = \frac{AI_0}{2\mu_b}\exp(-2\mu_s x \csc\theta) \tag{a.5}$$

For the physical situation we have here, in which after extended high temperature heat-treatments a porous surface layer of zirconia (phase 1) forms on a bulk material consisting of a porous two-phase mixture of zirconia (phase 1) and lithium metazirconate (phase 2), it is relevant to compare the intensities of strong reflections from both these phases to assess the growth of the zirconia surface layer over time.

Following the treatment by Cullity and Stock[27] for quantitative analysis of multicomponent systems by the direct comparison method, we can evaluate the ratio of the diffracted intensities I_1 and I_2 of two strong reflections from phases 1 and 2 respectively, from which we can determine effective volume fractions of the two phases to compare with the experimental measurements such as those in Fig. 12.

A zirconia reflection whose Bragg angle is θ_1 will have contributions from both the surface and bulk in proportion to the volume fractions $V_{1,s}$ and $V_{1,b}$ of the zirconia in these two regions, so that in general I_1 takes the form

$$I_1 = \frac{KR_1V_{1,b}}{2\mu_b}\exp(-2\mu_s x \csc\theta_1) + \frac{KR_1V_{1,s}}{2\mu_s} \times (1 - \exp(-2\mu_s x \csc\theta_1)) \tag{a.6}$$

where the first term represents the contribution to the intensity from the bulk and the second term represents the contribution from the surface layer. K is a constant, independent of the type and amount of the diffracting substance, while R_1 depends on θ_1, the indices of the set of diffracting planes hkl and the kind of substance (Eq. 12-10 of Cullity and Stock).

Likewise, the intensity from a lithium zirconate reflection whose Bragg angle is θ_2 will simply take the form

$$I_2 = \frac{KR_2V_{2,b}}{2\mu_b}\exp(-2\mu_s x\csc\theta_2) \quad \text{(a.7)}$$

where $V_{2,b}$ is the volume fraction of the lithium metazirconate in the bulk. In this case, there is no contribution to the intensity from the surface layer. The ratio of the intensity of I_1 and I_2 is therefore

$$\frac{I_1}{I_2} = \frac{R_1}{R_2}\left\{\frac{V_{1,b}}{V_{2,b}}\exp(2\mu_s x(\csc\theta_2 - \csc\theta_1))\right\} + \frac{R_1}{R_2} \times \left\{\frac{\mu_b}{\mu_s}\frac{V_{1,s}}{V_{2,b}}\exp(2\mu_s x\csc\theta_2)(1-\exp(-2\mu_s x\csc\theta_1))\right\} \quad \text{(a.8)}$$

and so if $x=0$, we recover Eq. 12-12 of Cullity and Stock. As the surface layer thickens, its contribution to the total intensity of the zirconia X-ray peak increases. Hence, the apparent level of zirconia, $V_{1,app}$, in the compact increases. From Eq. (a.8), we can determine this apparent level through the equation

$$\frac{I_1}{I_2} = \frac{R_1V_{1,app}}{R_2V_{2,app}} = \frac{R_1V_{1,app}}{R_2(1-V_{1,app})} \quad \text{(a.9)}$$

since in working out the apparent level of zirconia we can neglect porosity in the sample.

Using the values of mass absorption coefficients for Cu$K_{\alpha 1}$ radiation for Li, O and Zr of 0.5, 11.5 and 139 cm^2/gm from Volume C, Table 4.2.4.3 of the International Tables for Crystallography,[28] the mass absorption coefficients of ZrO_2 and Li_2ZrO_3 are calculated to be 106 and 86.5 cm^2/gm. Fully dense ZrO_2 and Li_2ZrO_3 ceramics have densities of 5.819 and 4.159 gm/cm^3 respectively, so that the linear absorption coefficients of fully dense ZrO_2 and Li_2ZrO_3, μ_1 and μ_2, are 615 and 360 cm^{-1}.

For a porous zirconia surface layer, the linear absorption coefficient, μ_s, is simply $V_{1,s}\ \mu_1$ since the volume fraction of porosity is $(1-V_{1,s})$. Likewise, the linear absorption coefficient of a porous two phase mixture of zirconia and lithium zirconate in which the volume fraction of porosity is $(1-V_{1,b}-V_{2,b})$ is $\mu_b = V_{1,b}\ \mu_1 + V_{2,b}\ \mu_2$. If both the surface region of porous ZrO_2 and the bulk region of porous ZrO_2 and Li_2ZrO_3 sampled by the X-rays were ideal polycrystalline samples without any texture, the parameters R_1 and R_2 in Eq. (a.8) would each be of the form

$$R = \frac{1}{V_{cell}^2}\left[|F_{hkl}|^2 p\left(\frac{1+\cos^2 2\theta}{\sin^2\theta\cos\theta}\right)\right]e^{-2M} \quad \text{(a.10)}$$

where V_{cell} is the volume of the unit cell, F_{hkl} is the structure factor of the *hkl* reflection, p is its multiplicity, the term in θ is the Lorentz polarisation factor and e^{-2M} is a temperature factor.[27] Calculated relative values of R for reflections for ideal polycrystalline samples of both ZrO_2 and Li_2ZrO_3 are given in the JCPDS files 86-1450 and 76-1150 respectively. The strongest Li_2ZrO_3 reflection is the 110 reflection at $2\theta = 20.286^\circ$. The strongest ZrO_2 reflections are the $\bar{1}11$ reflection at $2\theta = 28.183^\circ$ and the 111 reflection at $2\theta = 31.473^\circ$, with relative intensities of 1 and 0.677 respectively. Absolute comparisons of the intensities from Li_2ZrO_3 and ZrO_2 taking into account the sizes of the unit cells and the calculated values of F_{hkl} shows that the values of R from the 110 Li_2ZrO_3 reflection and the 111 ZrO_2 reflection should be almost equal. Thus, for a comparison of these reflections as the surface layer of zirconia grows, we can usefully take the ratio R_1/R_2 to be unity as a reasonable approximation for a semi-quantitative analysis of the growth of the zirconia surface layer, given the known texture of the zirconia within the pellets.

References

1. Vincent, C. A., Lithium batteries: a 50-year perspective 1959-2009. *Solid State Ionics*, 2000, **134**, 159–167.
2. Lu, C.-H. and Wei-Cheng, L., Reaction mechanism and kinetics analysis of lithium nickel oxide during solid-state reaction. *J. Mater. Chem.*, 2000, **10**, 1403–1407.
3. Broussely, M., Perton, F., Biensan, P., Bodet, J. M., Labat, J., Lecerf, A., Delmas, C., Rougier, A. and Pérès, J. P., Li_xNiO_2, a promising cathode for rechargeable lithium batteries. *J. Power Sources*, 1995, **54**, 109–114.
4. Subramanian, V., Chen, C. L., Chou, H. S. and Fey, G. T. K., Microwave-assisted solid-state synthesis of $LiCoO_2$ and its electrochemical properties as a cathode material for lithium batteries. *J. Mater. Chem.*, 2001, **11**, 3348–3353.
5. Yang, X., Tang, W., Kanoh, H. and Ooi, K., Synthesis of lithium manganese oxide in different lithium-containing fluxes. *J. Mater. Chem.*, 1999, **9**, 2683–2690.
6. Kudo, H., Okuno, K. and O'hira, S., Tritium release behaviour of ceramic breeder candidates for fusion reactors. *J. Nucl. Mater.*, 1988, **155–157**, 524–528.
7. Pfeiffer, H., Bosch, P. and Bulbulian, S., Sol-gel synthesis of $Li_2ZrSi_6O_{15}$ powders. *J. Mater. Chem.*, 2000, **10**, 1255–1258.
8. Pfeiffer, H., Bosch, P. and Bulbulian, S., Synthesis of lithium silicates. *J. Nucl. Mater.*, 1998, **257**, 309–317.
9. Johnson, C. E., Tritium behaviour in lithium ceramics. *J. Nucl. Mater.*, 1999, **270**, 212–220.
10. Montanaro, L., Negro, A. and Lecompte, J. P., Lithium metazirconate for nuclear application: physical and mechanical properties. *J. Mat. Sci.*, 1995, **30**, 4335–4338.
11. Nishikawa, M. and Baba, A., Tritium inventory in Li_2ZrO_3 blanket. *J. Nucl. Mater.*, 1998, **257**, 162–171.
12. Nagai, M., Hibino, M., Nishino, T. and Noda, K., Effect of γ-ray irradiation on Li_2O ceramics. *J. Mat. Sci. Lett.*, 1993, **12**, 107–109.
13. Kawamura, Y. and Nishikawa, M., Adsorption characteristics of water vapor on Li_2ZrO_3. *J. Nucl. Mater.*, 1995, **218**, 57–65.
14. Kutolin, S. A. and Druz, N. A., Effect of synthesis conditions on the structure and properties of lithium metazirconate. *Inorg. Mater.*, 1965, **1**, 1590–1592.
15. Hodeau, J. L., Marezio, M., Santoro, A. and Roth, R. S., Neutron profile refinement of the structures of Li_2SnO_3 and Li_2ZrO_3. *J. Solid State Chem.*, 1982, **45**, 170–179.
16. Wyers, G. P. and Cordfunke, E. H. P., Phase relations in the system Li_2O–ZrO_2. *J. Nucl. Mater.*, 1989, **168**, 24–30.

17. Sood, D. D., Dash, S. and Prasad, R., Phase diagram and thermodynamic calculations of alkali and alkaline earth metal zirconates. *J. Nucl. Mater*., 1996, **228**, 83–116.
18. Gualtieri, A., Norby, P., Hanson, J. and Hriljac, J., Rietveld refinement using synchrotron X-ray powder diffraction data collected in transmission geometry using an imaging-plate detector: application to standard *m*-ZrO_2. *J. Appl. Crystallogr*., 1996, **29**, 707–713.
19. Quintana, P., Leal, J., Howie, R. A. and West, A. R., Li_2ZrO_3: a new polymorph with the α-$LiFeO_2$ structure. *Mat. Res. Bull*., 1989, **24**, 1385–1389.
20. Castro-García, S., Julien, C. and Señarís-Rodríguez, M. A., Structural and electrochemical properties of Li–Ni–Co oxides synthesized by wet chemistry via a succinic-acid-assisted technique. *Inter. J. Inorg. Mater*., 2001, **3**, 323–329.
21. Thackeray, M. M., Mansuetto, M. F. and Johnson, C. S., Thermal stability of $Li_4Mn_5O_{12}$ electrodes for lithium batteries. *J. Solid State Chem*., 1996, **125**, 274–277.
22. Antolini, E. and Ferretti, M., Synthesis and thermal stability of $LiCoO_2$. *J. Solid State Chem*., 1995, **117**, 1–7.
23. Kingery, W. D., Bowen, H. K. and Uhlmann, D. R., *Introduction to Ceramics*, Second edition. Wiley-Interscience, New York, 1976, pp. 469–490.
24. Mendelson, M. I., Average grain size in polycrystalline ceramics. *J. Am. Ceram. Soc*., 1969, **52**, 443–446.
25. Goldstein, J. I., Newbury, D. E., Echlin, P., Joy, D. C., Fiori, C. and Lifshin, E., *Scanning Electron Microscopy and X-ray Microanalysis*. Plenum, New York, 1981, pp. 75–77.
26. Ohring, M., *The Materials Science of Thin Films*. Academic Press, San Diego, 1992, pp. 227–232.
27. Cullity, B. D. and Stock, S. R., *Elements of X-ray Diffraction, Third Edition*. Prentice Hall, NJ, 2001, pp. 152–154 and pp. 347–352.
28. Wilson, A. J. C., ed., *International Tables for Crystallography*, 4th revised edition, Volume C. Kluwer Academic Publishers, Dordrecht, 1995, pp. 200–202.